Electronic Supplementary Material (ESI) for Journal of Materials Chemistry A.

Supporting information

"Pea-pod-like" Nitrogen-doped Hollow Porous Carbon Cathode Hosts Decorated with Polar Titanium Dioxide Nanocrystals as Efficient Polysulfide Reservoirs for Advanced Lithium-Sulfur batteries

Weiqi Yao[a], Chenjie Chu[a], Weizhong Zheng[a], Liang Zhan[a,b*] and Yanli Wang[a*]

[a]State Key Laboratory of Chemical Engineering, Key Laboratory for Specially Functional Polymers and Related Technology of Ministry of Education, Shanghai Key Laboratory of Multiphase Materials Chemical Engineering, East China University of Science and Technology, Shanghai 200237, China;

[b]CAS Key Laboratory of Carbon Materials, Institute of Coal Chemistry, Chinese Academy of Sciences, Taiyuan 030001, China.

[*]Corresponding authors: Liang Zhan, E-mail: zhanliang@ecust.edu.cn；Yanli Wang, E-mail: ylwang@ecust.edu.cn

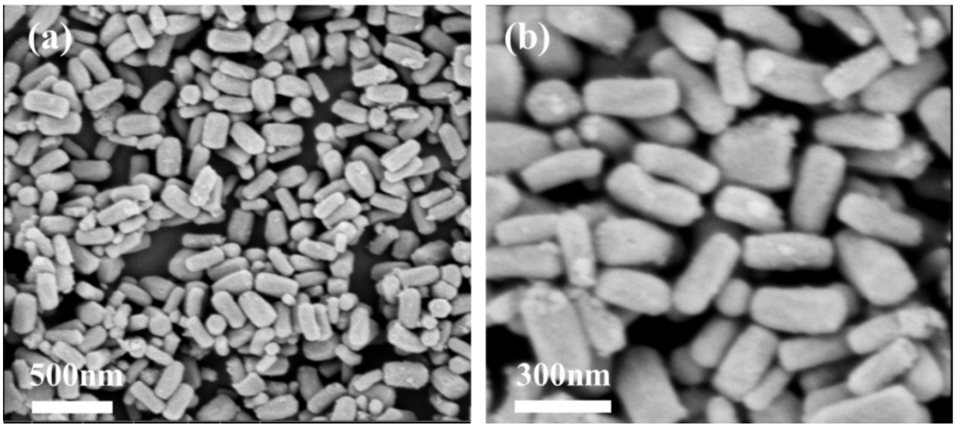

Figure S1. SEM images of the porous rod-SiO_2.

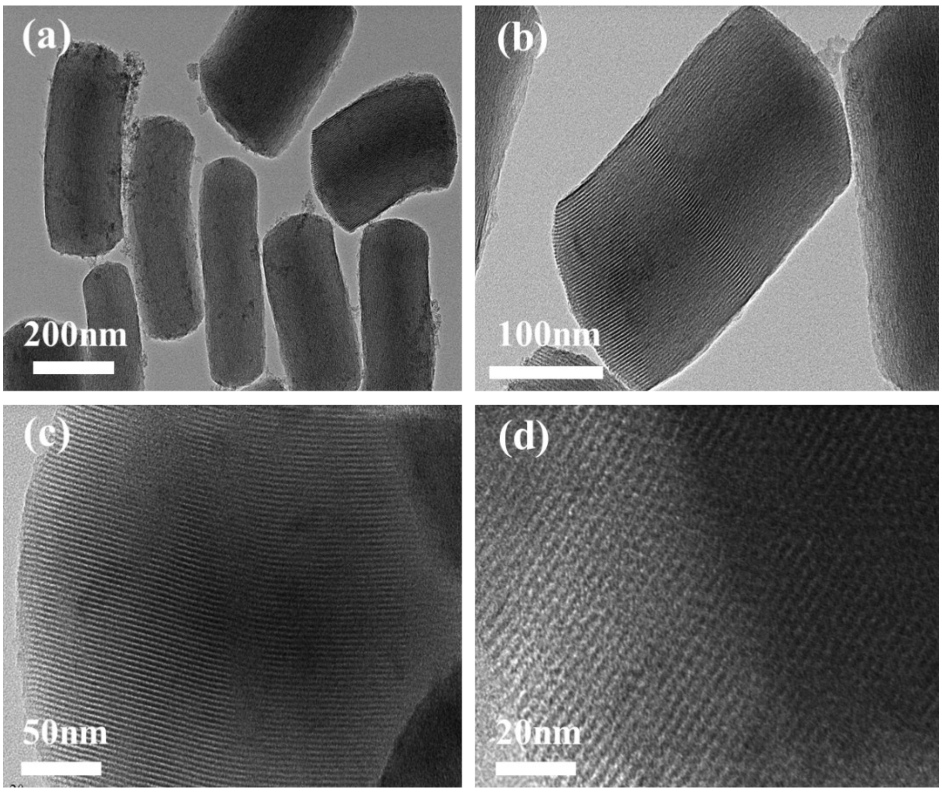

Figure S2. TEM images of the porous rod-SiO_2.

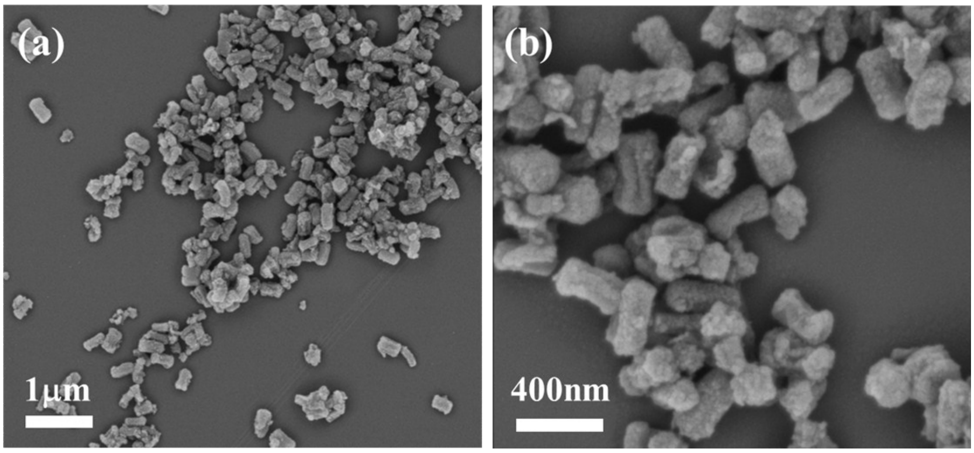

Figure S3. SEM images of the rod-C after etching off silica by NaOH solution.

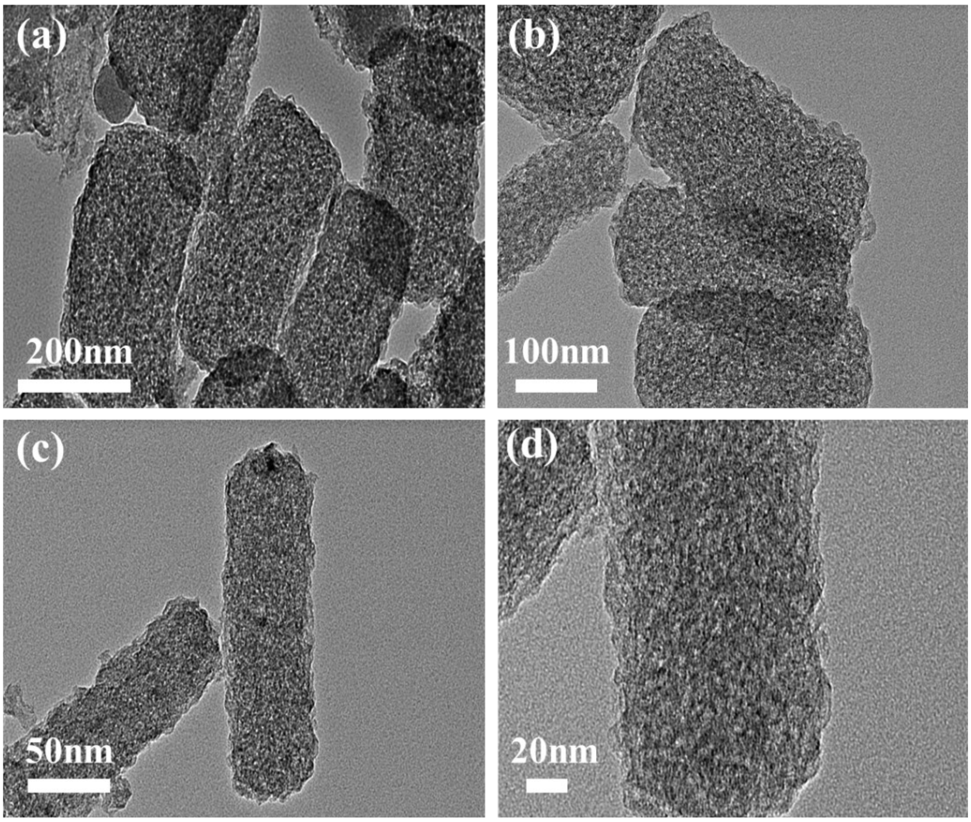

Figure S4. TEM images of the porous rod-C after etching off silica by NaOH solution.

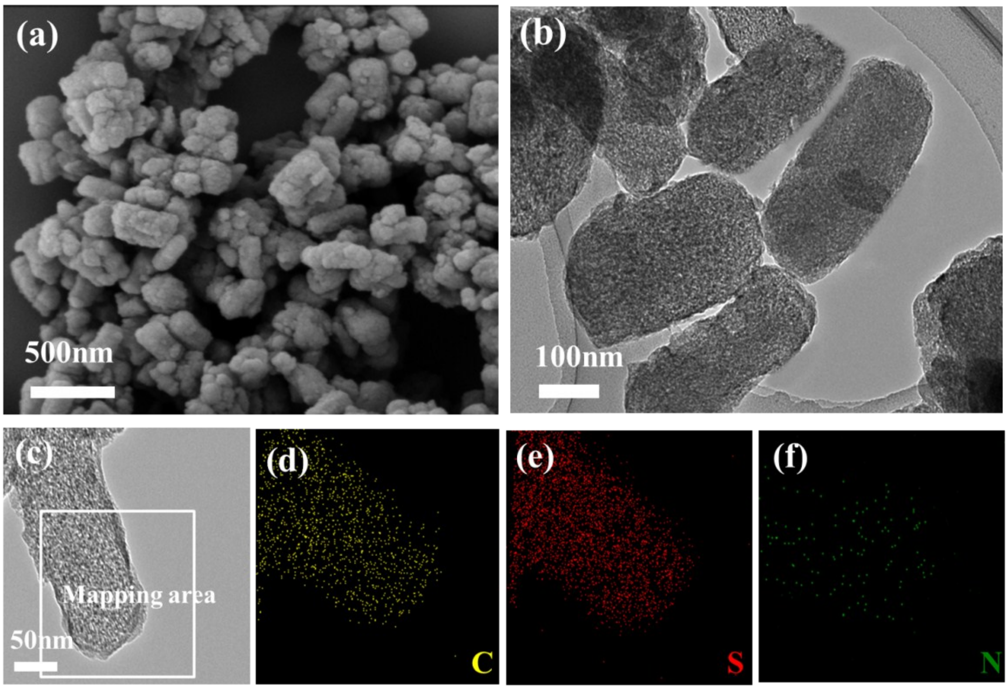

Figure S5. SEM image (a), TEM image (b), STEM Bright field image (c) of rod-C/S and its corresponding elemental mapping images of carbon (d), sulfur (e) and nitrogen (f).

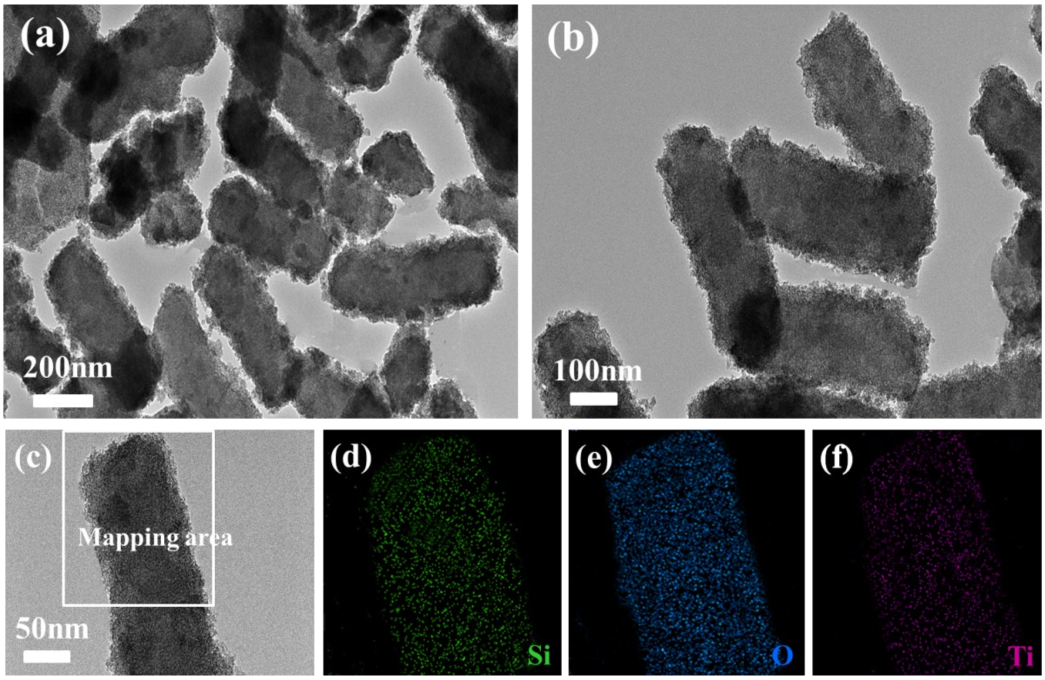

Figure S6. TEM image (a,b), STEM Bright field image (c) of rod-SiO_2@TiO_2 and its corresponding elemental mapping images of silicon (d), oxygen (e) and titanium (f).

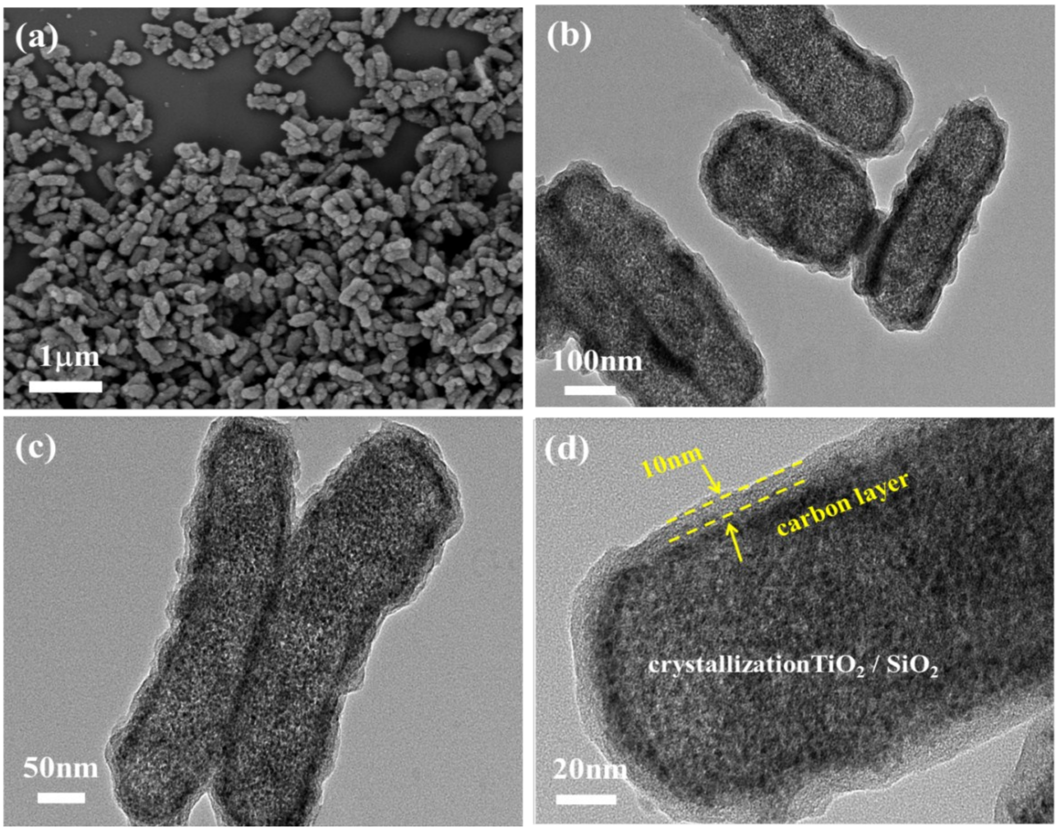

Figure S7. SEM (a) and TEM images (b, c, d) of the rod-SiO_2@TiO_2@C before etched off SiO_2.

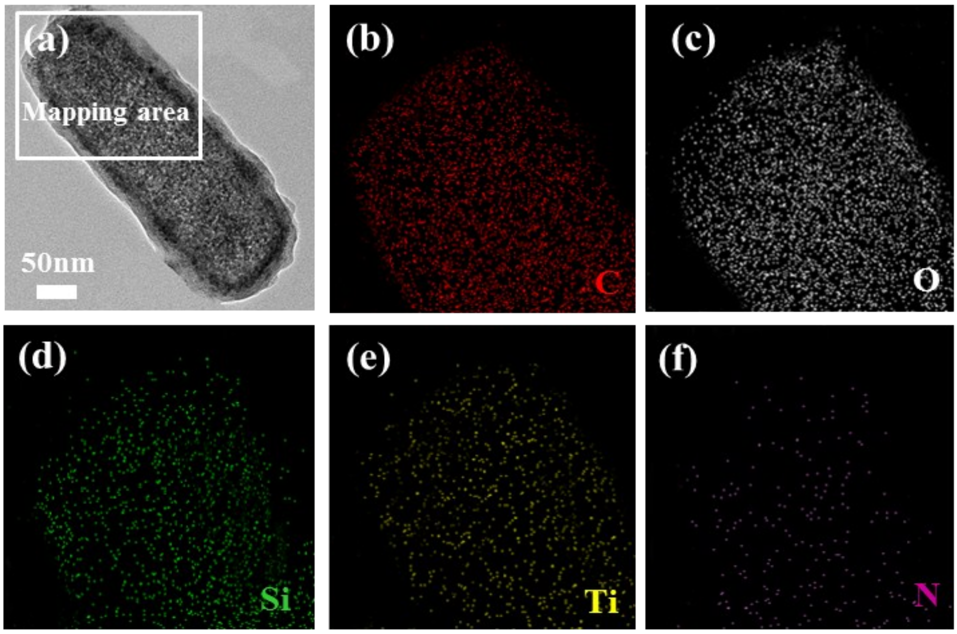

Figure S8. STEM Bright field image (a) of rod-SiO_2@TiO_2@C before etched off SiO_2 and its corresponding elemental mapping images of carbon (b), oxygen (c), silicon (d), titanium (e) and nitrogen (f).

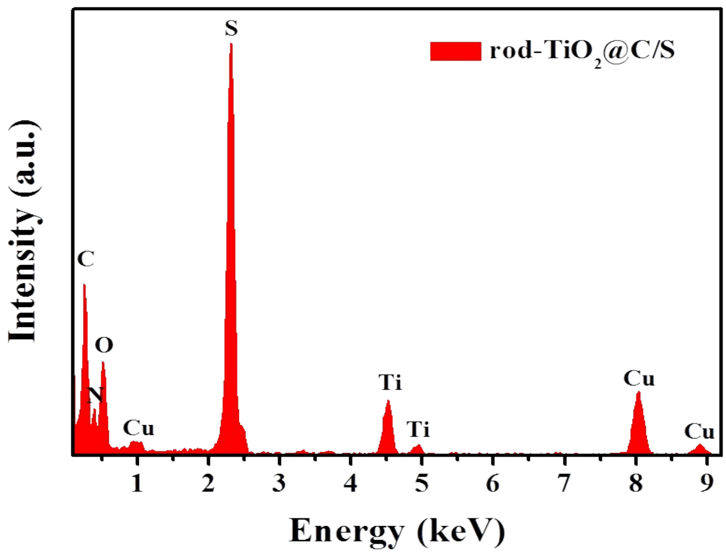

Figure S9. EDS spectrum of the rod-TiO_2@C/S.

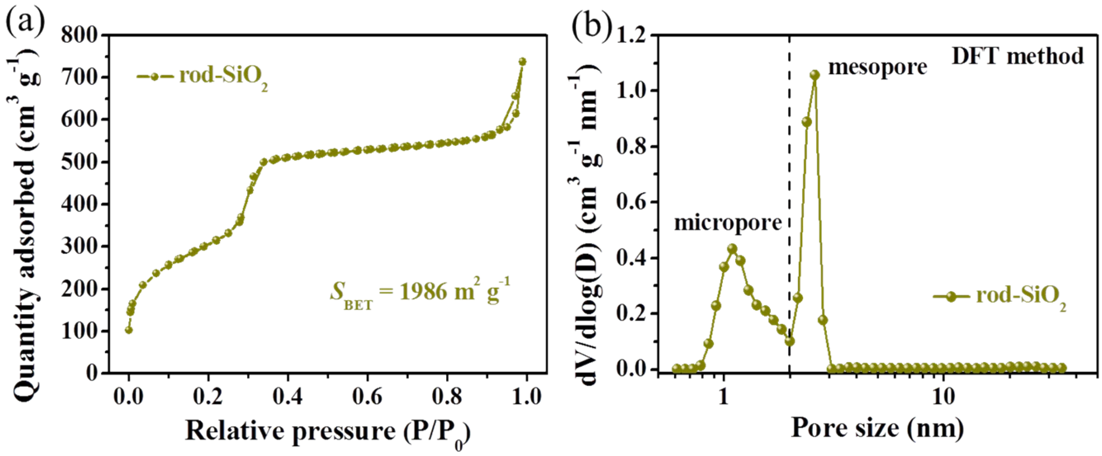

Figure S10. Nitrogen adsorption-desorption isotherms (a) and the corresponding pore size distributions (b) of porous rod-SiO_2.

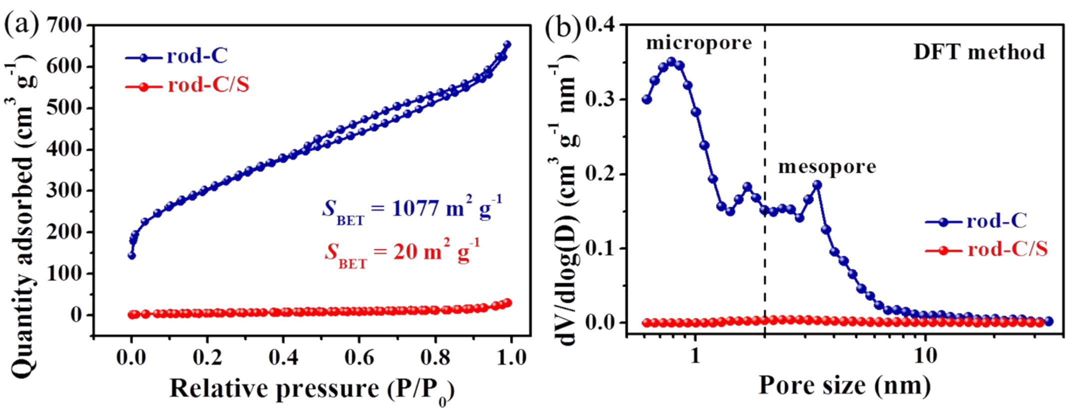

Figure S11. Nitrogen adsorption-desorption isotherms (a) and the corresponding pore size distributions (b) of rod-C and rod-C/S.

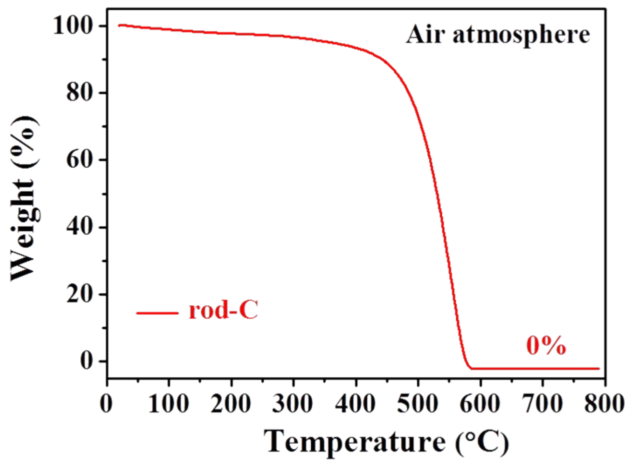

Figure S12. TG curves of rod-C under air atmosphere.

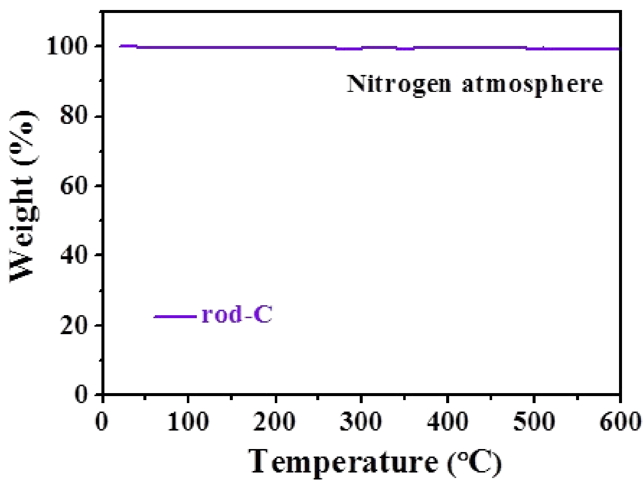

Figure S13. TG curves of rod-C under nitrogen atmosphere.

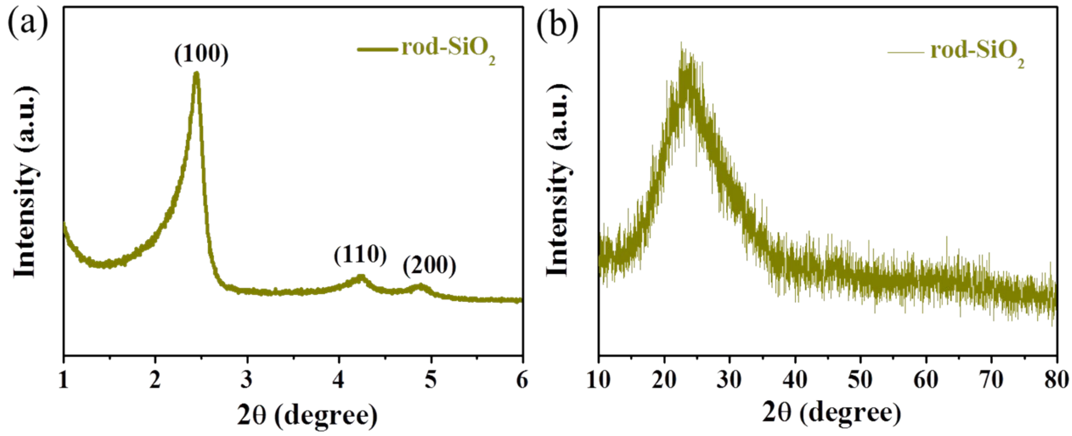

Figure S14. Small angle (a) and wide angle (b) XRD pattern of the rod-SiO_2.

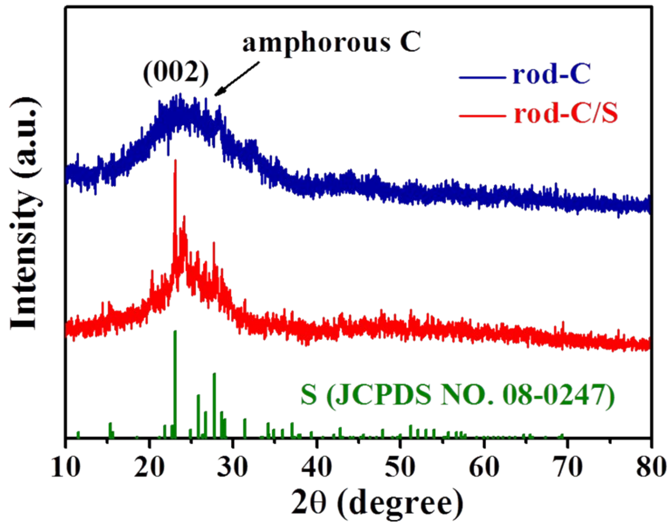

Figure S15. XRD patterns of rod-C and rod-C/S.

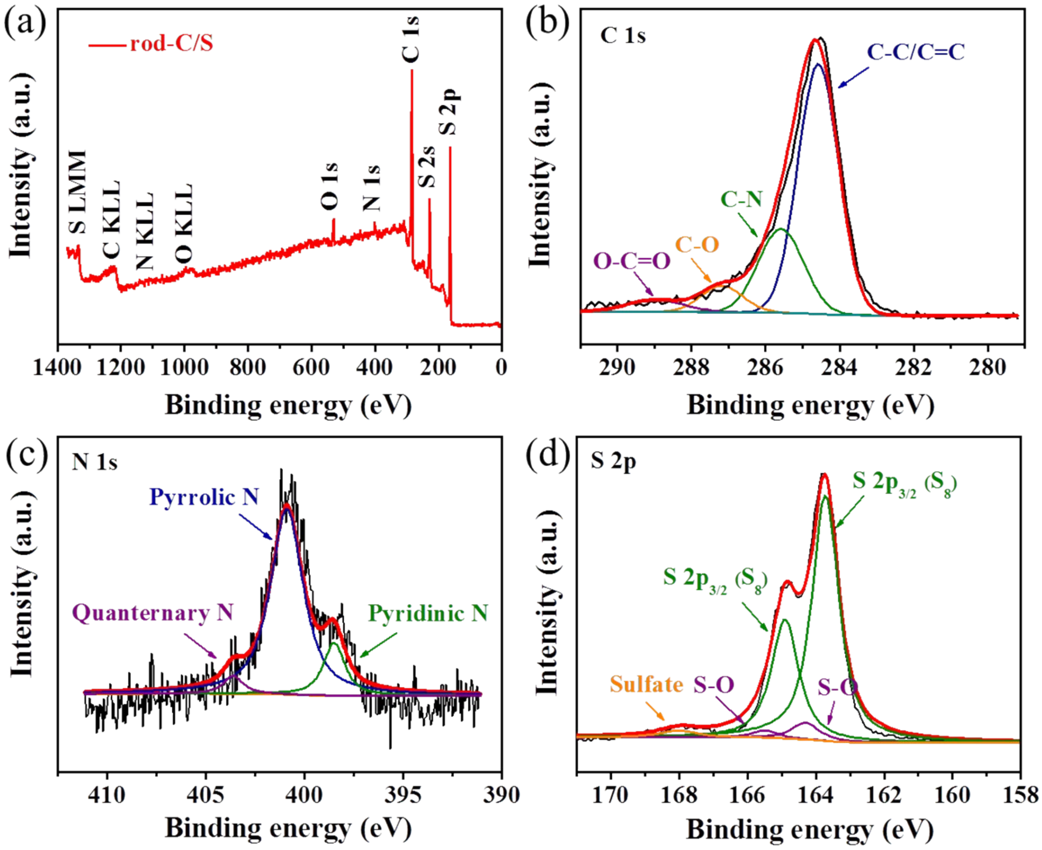

Figure S16. XPS full spectrum (a), the deconvoluted C 1s (b), N 1s (c) and S 2p (d) of rod-C/S.

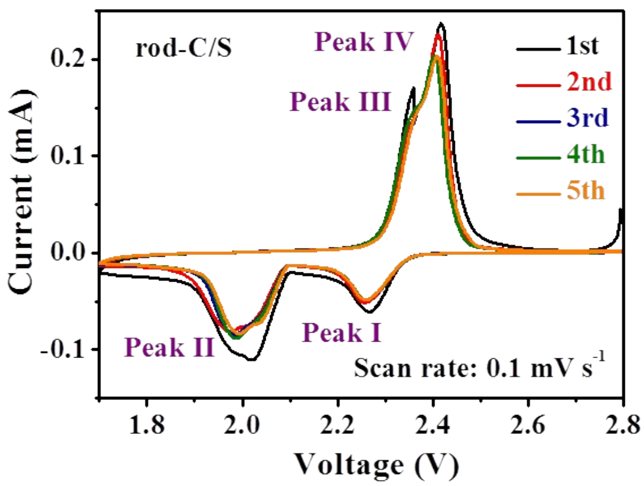

Figure S17. Representative CV curves of the first five cycles for rod-C/S cathodes at a scan rate of 0.1 mV s^{-1}.

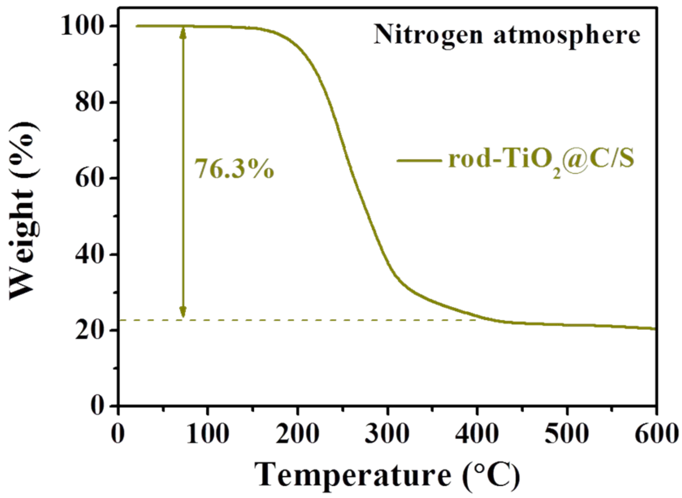

Figure S18. TG curve of rod-TiO_2@C/S under nitrogen atmosphere, the sulfur content is about 76.3%.

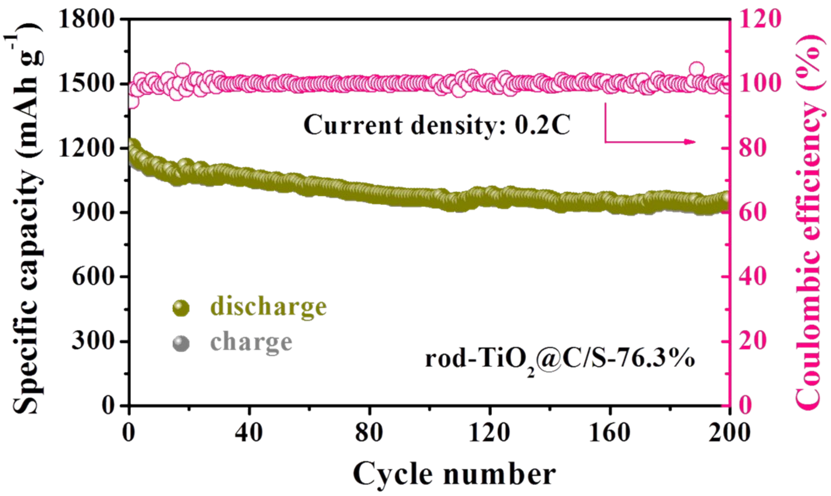

Figure S19. Cycle performance of the rod-TiO_2@C/S cathodes at the current density of 0.2C, the sulfur content is about 76.3%.

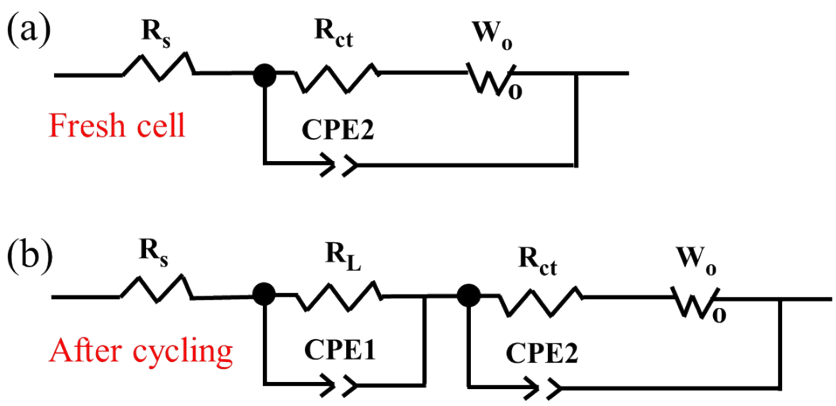

Figure S20. The EIS equivalent circuits of rod-C/S and rod-TiO_2@C/S cathodes for Li-S batteries, while (a) is suitable for the fresh cell without the process of R_L and its relevant CPE1, (b) can be utilized to the cell after cycling.

R_s: The resistance of the electrolyte;

R_L: The resistance of the solid electrolyte interface (SEI) layer related to the insoluble Li_2S_2/Li_2S;

R_{ct}: The charge-transfer resistance, related to the electrode reaction kinetics;

CPE: The corresponding constant phase element;

Z_w: The semi-infinite Warburg diffusion impedance of long-chain LiPSs.

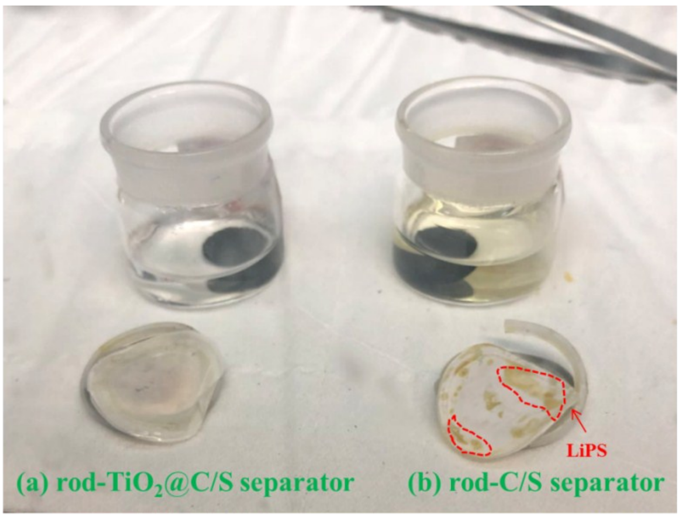

Figure S21. Digital photos of the separators after 200 cycles half-cell at 0.2C for rod-TiO_2@C/S (a) and rod-C/S (b) cathodes, and then immersed in DOL solvent.

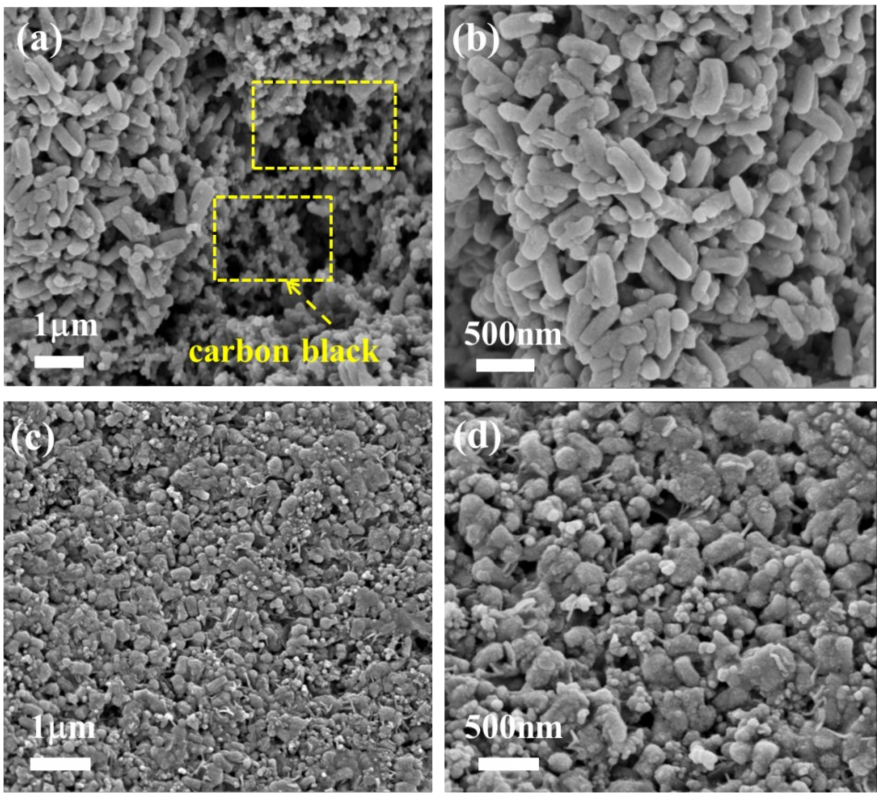

Figure S22. SEM images of the rod-TiO_2@C/S (a,b) and rod-C/S (c,d) cathodes after 200 cycles at 0.2C.

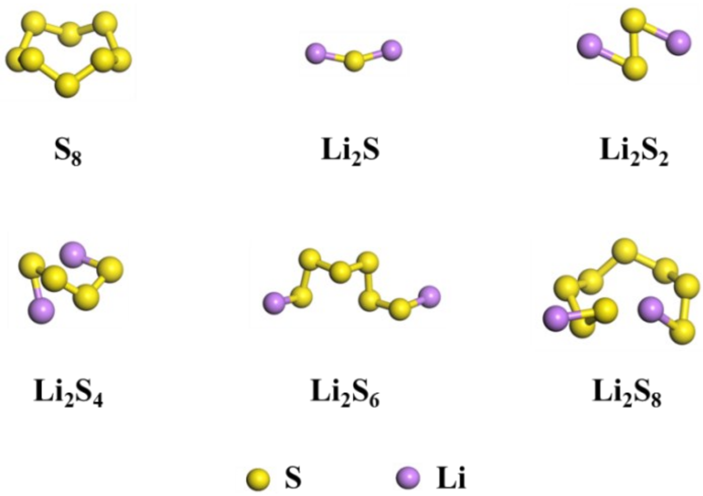

Figure S23. The optimize structures of S_8 and lithium polysulfides.

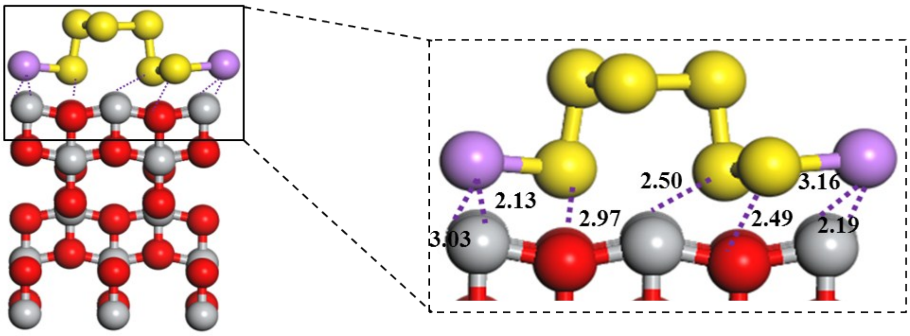

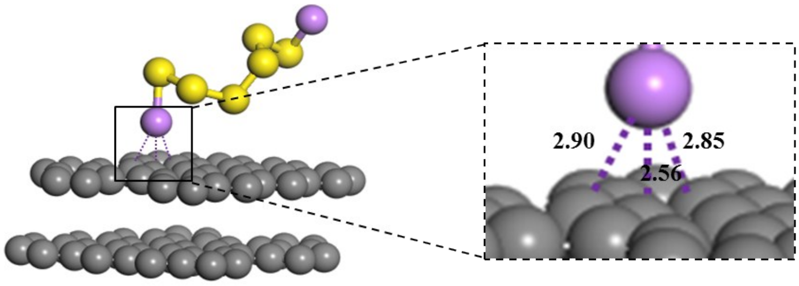

Figure S24. The geometric configurations and binding energies of a Li_2S_6 molecular with carbon host materials and TiO_2.

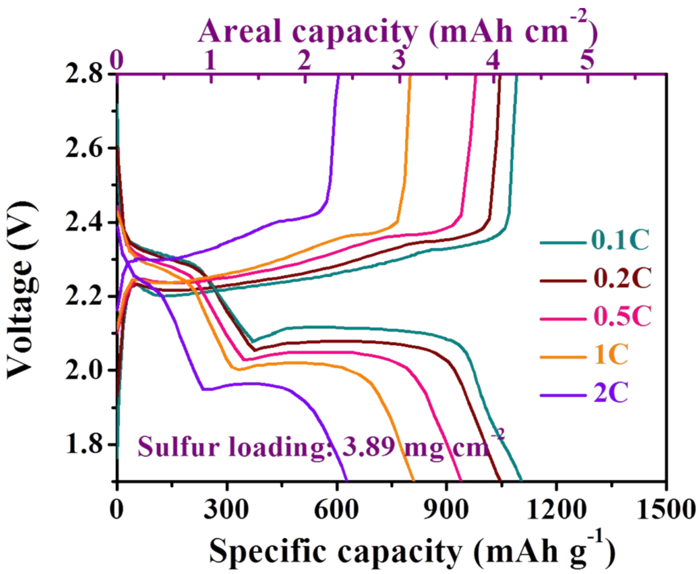

Figure S25. Galvanstatic discharge-charge voltage profiles of rod-TiO_2@C/S cathodes at various current rates under 3.89 mg cm^{-2} sulfur mass loading for Li-S batteries.

Table S1. The detailed pore structures of the as-prepared samples.

Sample	Specific surface area (S_{BET}, m^2 g^{-1})	Total pore volume (V, cm^3 g^{-1})	Average pore size (nm)
rod-SiO_2	1986	1.14	2.3
rod-C	1077	1.01	3.8
rod-TiO_2@C	757	0.91	4.8
rod-C/S	20	0.05	-
rod-TiO_2@C/S	19	0.03	-

Table S2. Impedance parameters of the EIS spectra for rod-C/S and rod-TiO_2@C/S cathodes before cycling.

Sample	R_s (Ω)	R_{ct} (Ω)
rod- TiO_2@C/S	4.16	24.74
rod-C/S	4.68	29.17

Table S3. Impedance parameters of the EIS spectra for rod-C/S and rod-TiO_2@C/S cathodes after 200 cycles at 0.2C.

Sample	R_s (Ω)	R_L (Ω)	R_{ct} (Ω)
rod- TiO_2@C/S	2.37	11.49	15.05
rod-C/S	7.93	34.73	51.21

Table S4. The cycle performance comparisons of rod-TiO_2@C/S cathode materials for Li-S batteries with other representative cathodes (utilizing carbon/metal oxide or metal sulfide nanocomposites as efficient polysulfide immobilizer) from previous reported literatures.

Sample	Sulfur content (%)	Sulfur mass loading (g cm^{-2})	Current density (C)	Cycles	Initial/highest capacity (mAh g^{-1})	Reversible capacity (mAh g^{-1})	Capacity retention (%)	Capacity decay per cycle (%)
This work (rod-TiO_2@C/S)	**65.4**	**1.7-2.0**	**0.2**	**200**	**1248**	**1017**	**81.5**	**0.0925**
			0.5	**500**	**1128**	**853**	**75.6**	**0.0488**
			1	**1500**	**1031**	**728**	**70.6**	**0.0196**
			2	**1500**	**943**	**604**	**64.1**	**0.0240**
		4.04	**0.5**	**300**	**921**	**683**	**74.2**	**0.0861**
C@TiO_2@C-S[1]	76.4	2.5	0.5	300	999	740	74.1	0.0864
			2	500	774	511	66.0	0.0680
NbS_2@S@IG[2]	72.0	1.05	0.5	350	1185	856	72.2	0.0793
		3.25	1	600	506	405	80.0	0.0333
S-PPy-MnO_2[3]	70.0	1	0.2	200	1420	985	69.4	0.1532
			1	500	850	550	64.7	0.0706
MoO_2/G-S[4]	79.0	-	0.2	100	1124	905	80.5	0.1948
			1	500	806	664	82.4	0.0352
MoS_{2-x}/rGO/S[5]	76.0	1.5	0.5	600	1251	628	50.2	0.0830
S/NiS@C-HS[6]	73.7	1.0	0.2	200	1002	718	71.7	0.1417
		2.3	0.5	300	723	695	96.1	0.0129
Fe_2O_3-PGM-S[7]	60	1	0.2	100	1124	905	80.5	0.1948
			1	500	806	664	82.4	0.0352
N-Co_3O_4@N-C/rGO-S[8]	75	2.13	0.2	300	1223	945	77.3	0.0758
			2	1000	-	611	-	-

	5.89	0.2	500	-	568	-	-

Table S5. The rate capability comparisons of rod-TiO_2@C/S cathode material for Li-S batteries with other representative cathodes (utilizing carbon/metal oxide or metal sulfide nanocomposites as efficient polysulfide immobilizer) from previous reported literatures.

Sample	**Sulfur content (%)**	**Sulfur mass loading (g cm^{-2})**	**Current density (C)**	**Reversible capacity (mAh g^{-1})**
This work (rod-TiO_2@C/S)	**65.4**	**1.7-2.0**	**5**	**717**
			8	**605**
			10	**509**
		3.89	**2**	**627**
C@TiO_2@C-S[1]	76.4	2.5	2	774
NbS_2@S@IG[2]	72.0	1.05	3	910
			5	~600
			10	~450
		3.25	1	~500
S-PPy-MnO_2[3]	70.0	1	4	350
MoO_2/G-S[4]	79.0	-	2	615
MoS_{2-x}/rGO/S[5]	76.0	1.5	8	827
S/NiS@C-HS[6]	73.7	1.0	2	674
Fe_2O_3-PGM-S[7]	60	1	5	565
N-Co_3O_4@N-C/rGO-S[8]	75	2.13	2	756
			3	652

References for the Supporting Information

1 M. Fang, Z. Chen, Y. Liu, J. Quan, C. Yang, L. Zhu, Q. Xu, *J. M. Chem. A*, 2018, **6**, 1630-1638.

2 Z. Xiao, Z. Yang, L. Zhang, H. Pan and R. Wang, *ACS Nano*, 2017, **11**, 8488-8498.

3 J. Zhang, Y. Shi, Y. Ding, W. Zhang, G. Yu, *Nano Lett.*, 2016, **16**, 7276-7281.

4 X. Wu, Y. Du, P. Wang, L. Fan, J. Cheng, M. Wang, Y. Qiu, B. Guan, H. Wu, N. Zhang and K. Sun, *J. M. Chem. A*, 2017, **5**, 25187-25192.

5 H. Lin, L. Yang, X. Jiang, G. Li, T. Zhang, Q. Yao, G. Zheng and J. Lee, *Energy Environ. Sci.*, 2017, **10**, 1476-1486.

6 C. Ye, L. Zhang, C. Guo, D. Li, A. Vasileff, H. Wang and S. Qiao, *Adv. Funct. Mater.*, 2017, **27**, 1702524.

7 C. Zheng, S. Niu, W. Lv, G. Zhou, J. Li, S. Fan, Y. Deng, Z. Pan, B. Li, F. Kang, Q. Yang, *Nano Energy*, 2017, **33**, 306-312.

8 J. Xu, W. Zhang, Y. Chen, H. Fan, D. Su and G. Wang, *J. Mater. Chem. A*, 2018, **6**, 2797-2807.